Sensitivity Analysis of Earth Fault Localization based on Voltage Signatures in Medium Voltage Grids

Wormann, Julian; Tafehi, Ehsan ; Duchon, Markus; Silva, Nuno; Schwefel, Hans-Peter Christian

Published in:
ICC 2021 - IEEE International Conference on Communications

DOI (link to publication from Publisher):
10.1109/ICC42927.2021.9500802

Publication date:
2021

Document Version
Early version, also known as pre-print

Sensitivity Analysis of Earth Fault Localization based on Voltage Signatures in Medium Voltage Grids

Julian Wörmann
fortiss GmbH
Munich, Germany
woermann@fortiss.org

Ehsan Tafehi
GridData GmbH
Traunstein, Germany
tafehi@griddata.eu

Markus Duchon
fortiss GmbH
Munich, Germany
duchon@fortiss.org

Nuno Silva
GridData GmbH
Traunstein, Germany
nuno.silva@griddata.eu

Hans-Peter Schwefel
GridData GmbH & Aalborg University
Traunstein, Germany & Aalborg, DK
schwefel@griddata.eu

***Abstract*—Fast localization of earth faults in medium voltage grids is required in order to avoid subsequent faults and to quickly restore the normal grid operation. This paper builds upon an approach to localize earth faults by signature matching of high-resolution voltage measurements from the primary substation. The signatures are generated from a simulation model, for which in practice not all parameters are accurately known. Therefore, it is necessary to understand the impact of deviations of these parameters on the signature comparison in the localization approach. This paper presents an approach for performing such sensitivity analysis and shows the results using simulations of a realistic small medium voltage grid.**

***Index Terms*—fault localization, electricity distribution grids, signature comparison, sensitivity analysis,**

I. Introduction

An electrical fault is an abnormal condition, caused by equipment failures such as transformers, human errors or environmental conditions. Faults in power system networks can result in severe economic losses and reduce the reliability of the electrical system [10].

An earth fault is a fault, where the power carrying cable or conductor gets into contact with earth or with any conducting material in contact with earth. Locating earth faults in electrical distribution grids is essential to the operation of the electrical grid. With the localization of an occurring earth fault, technical teams can be dispatched to resolve the fault, normally by repairing a failed grid component or link. Obviously, visual inspection by human technicians is not feasible, given that an electrical distribution grid can encompass underground cables or tens of kilometers of overhead lines, and the time to repair the fault is critically important.

The existing protection system at the primary (HV/MV) substation can detect the occurrence of earth faults, but not their locations. The deployment of Petersen coils in so-called compensated MV grids allows the continued operation of the grid despite the fault. However, the grid is not operating in the optimized conditions any more with consequences of lifetime reductions of electrical components and often resulting in subsequent faults, which then cause power outages at customers.

In order to localize the earth fault in a compensated MV grid, currently Distribution System Operators (DSOs) perform a sequence of switching operations to delimit the part of the MV grid, in which the fault likely has occurred, with manual inspection of the lines as a final localization step. This localization procedure is inefficient with respect to localization time and staff effort and prone to cause subsequent faults. Thus, there is a need for methods for locating earth faults in electrical distribution grids, in particular in compensated electrical distribution grids. Approaches in the literature use dedicated measurement hardware [4], [6] and active components that send signals through the cables [2] and are therefore expensive and show a high deployment barrier. Other techniques for fault location rely on specific analysis of the initial stage of fault transient [11] or inspection of traveling wave characteristics [8]. Machine Learning approaches for precise detection and localization have been also used [1], [8]. However, data acquisition for the training of reliable models is a serious challenge in real world scenarios. For an overview of employed methods, the reader is also referred to [3].

A novel data-driven approach to localize earth faults based on high-resolution measurements at the primary substation utilizing fault signatures has been recently published [9]. Such approach requires to generate fault signatures at different locations and with different parameterization from a transient grid simulation model. In order create such signature databases, it is important to understand which parameters influence the localization approach.

This paper provides a methodology in order to analyze this sensitivity and applies it to a realistic small example grid. In particular, we are interested in the range of different grid

This work has been cofinanced by the German Federal Ministry of Education and Research (BMBF) as part of the project 01IS18089A EDaF.

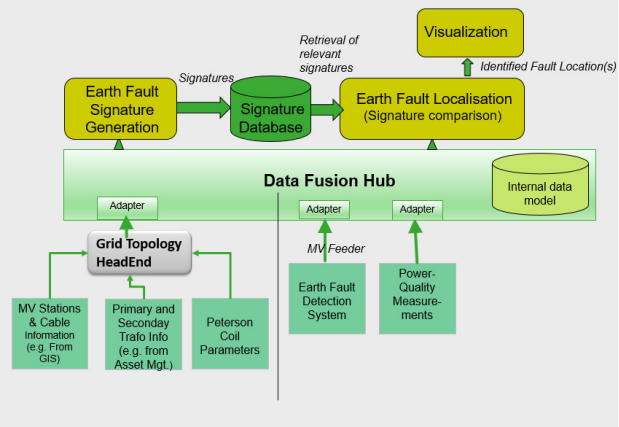

Fig. 1. Architecture of the Earth-Fault Localization Solution.

parameters, such that a robust signature based localization is still possible. For this purpose, we identified eight different scenarios where we assess the impact of different parameter scalings on the signatures by means of simple correlation measures. Our key observations are that the signatures are mostly robust against modifications of the loads, of the parameters of the Petersen Coil and of the power source; on the other hand, variations in the line/cable parameters lead to significant changes in the appearance of the signatures. The results of this sensitivity analysis pave the way for a successful application of the signature-based Earth Fault Localization to practical scenarios.

Section II introduces the basic architecture and components of the signature-based earth-fault localization approach. Section III describes the methodology how to analyze parameter sensitivity. This methodology is applied to a realistic small MV grid in Section IV. Finally, the results are summarized in Section V.

II. Signature-based Earth Fault Detection Method

The basic architecture of the signature based Earth Fault Localization is shown in the upper part of Figure 1. As any signature based method, it consists of two stages: (1) The Signature Generation function creates a set of signatures for different fault locations and for other potentially unknown or varying relevant parameters. These signatures are stored in a Signature Database (DB). This signature generation can occur in advance, e.g. triggered by major changes of the grid topology, which occur on timescales of several months. The basic approach for signature generation is explained further in a subsequent paragraph. (2) When an earth fault occurs, it will be signaled by the Earth Fault Detection system [7] and the Localization module will retrieve the high-resolution measurement of per-phase voltage measured at the primary substation in order to compare it with the signatures in the signature DB. The set of closest signatures and information about the corresponding fault locations that were causing these signatures are then used as the localization results.

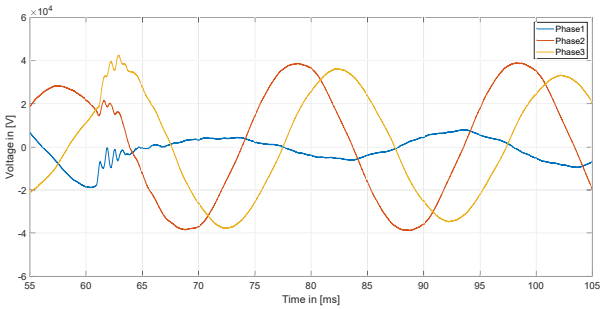

Fig. 2. Example measurement at a primary substation busbar, in which an Earth Fault occurs at Phase 1 after approx. 61ms.

The lower half of Figure 1 also illustrates the architecture that is utilized to obtain the required input data. Without going into detail in this paper, the architecture uses an intermediate layer for topology and measurement data interfacing and normalization of data representations.

Figure 2 visualizes the voltage signals of an actual earth fault measurement from a 30kV MV grid. The measurement has been taken by a Power-Quality Measurement device placed at the MV side of the primary substation (which in this case contained a 110kV/30kV transformer). The earth fault occurred on Phase 1, shown in blue in the figure. As a consequence of the earth fault, the Phase 1 voltage is strongly reduced, while Phase 2 and Phase 3 voltages increase, as the neutral point has been shifted towards the level of Phase 1. All three voltage signals show some particular behavior within a window of several milliseconds (ms) after the fault. In [9], the authors demonstrated that the shape of the voltage curve in these few ms after the fault is influenced by the fault location (and by the fault impedance). Therefore, the shape of the voltage signals within a few ms after the fault is used in order to localize the fault by comparing with signatures generated for different fault locations and fault resistances.

In order to localize the fault, voltage signatures are required from faults that occur at different locations in the grid. Such fault signatures are created by a detailed simulation model using Matlab/Simulink/Simscape Electrical with the following components:

- Model of the high-voltage grid by a voltage source
- Primary Transformer Model
- Petersen Coil
- Cables or overhead lines connecting the MV stations according to the grid topology (π model)
- Secondary Transformers
- Loads (constant P and Q, connected to the secondary transformers)

Except for the loads, the parameters of these components can be obtained from detailed grid component information that the distribution operator typically has available in electronic form; however, typically spread over different IT systems, e.g. SCADA system, GIS system, Asset Management System. The loads themselves could be measured by measurement devices in the secondary substation; however, this requires a large

amount of measurement points, and very few DSOs have deployed those so far. Therefore, loads in almost all cases need to be estimated.

Whenever an earth fault occurs, the most likely location in the grid is determined via comparing the correlation between the measured signals and the stored signatures from the DB. Crucial factors of this approach are signatures that are distinctive, robust to external factors and that can be processed efficiently, i.e. the number of signatures needed for accurate and fast localization that have to be stored in the database should be as low as possible. The first two aspects are further examined in the subsequent section.

III. Sensitivity Analysis Approach

Besides earth fault resistances, several other parameters of the grid topology will influence the shape and appearance of the measured signals. The aim of the subsequent sensitivity analysis is to show and assess the impact of different parameter settings on the generated voltage signatures. Invariance to certain parameters allows for a robust signature based localization since variations in these parameters or incomplete grid topology information can be simply neglected. On the other hand, identifying parameters that will influence the signal characteristics is a crucial step towards the creation of discriminative signal representations that enable fast and accurate fault localization.

A. Parameter Space

In Table I the different scenarios that have been examined are introduced. For each of the scenarios, the associated parameters and units are listed. For example the first row of Table I considers the case of varying loads. The corresponding parameters under investigation are the active power P and reactive power Q. The third column lists the initial values, i.e., $P = 100\,\text{kW}$ and $Q = 50\,\text{kvar}$, which are assumed to represent the ground truth in the sensitivity analysis. In the last column of Table I the used scaling factors are shown, e.g. the scaling factor $(1.0, 2.0)$ indicates that the the active power P is multiplied with the first factor 1.0, while the reactive power Q is scaled with factor 2.0. Eventually, in the subsequent sensitivity analysis we investigate the impact of these scalings on the signature characteristics. As a result, we will be able to assess the robustness of the signature based localization approach to certain parameter variations.

B. Analysis Approach

Since we are interested in an accurate localization, for each of the scenarios different earth fault locations are simulated and compared. Besides varying locations, different fault resistances have been simulated, too. In order to compare signatures generated at different fault locations and with varying parameter settings, the pairwise correlation coefficient is used [5]. To put things formally, given the matrix $S \in \mathbb{R}^{n\times m}$, composed of m signatures, each of dimension n, the covariance between the k-th and l-th signature is computed via

$$c(k,l) = \frac{1}{n-1}(s_k - \bar{s}_k)^\top (s_l - \bar{s}_l), \tag{1}$$

where $\bar{s}_k$ and $\bar{s}_l$ denote the mean of s_k and s_l, respectively. Finally, the correlation coefficient $r(k,l)$ between the k-th and l-th signature is calculated via

$$r(k,l) = \frac{c(k,l)}{\sqrt{c(k,k)\cdot c(l,l)}}. \tag{2}$$

The correlation coefficient takes values in the range $[-1, 1]$, with $|r(k,l)| = 1$ meaning perfect correlation and $r(k,l) = 0$ indicating no linear correlation.

The considered signals are assumed to have a resolution of $10\mu s$, i.e. one period (at 50Hz) is represented by 2000 samples. Such high-resolution measurements are obtained from Power-Quality measurement devices connected to the MV side of the primary substation, which in current practical deployments typically are configured to sampling frequencies between $10kHz$ and $100kHz$. For the sensitivity analysis, only the voltage of Phase 1, i.e. the phase that is connected to ground in the fault scenario is used. A fault is detected if the absolute voltage of the neutral in the three-phase system is above a certain threshold. This is in accordance to a typical real-world measurement process. The considered time window is set to $10ms$ after the fault is detected. Afterwards some minor preprocessing steps are performed. First, the maximum absolute value of the resulting signature is normalized to 1. Afterwards, the sign of the signatures is adjusted such that the signatures always start in the positive voltage regime, i.e. signatures with negative first sample are inverted.

C. Sensitivity Metric

The definition of a sensitivity metric will allow us to state an insensitivity range that reflects the impact of the parameter to the signature characteristics. In each scenario, it is assumed that the true parameters are known, i.e. the first factor represents the signature generated with the initial true parameter set. A signature is considered robust against variations in the parameter under consideration, if the correlation coefficient between the signatures within the same fault location is higher than the correlation coefficients obtained with signatures from some other location. To be precise, let $\hat{r}$ denote the correlation between the signature generated with the true parameters and the signature at the same fault location but with adjusted parameters according to the factors listed for each scenario. For each of the different factors, the number of signatures from other fault locations whose correlation is higher than $\hat{r}$ are identified. If this number exceeds a certain percentage, the factor is considered significant and thus limits the insensitivity range.

IV. Application of Sensitivity Analysis

The sensitivity analysis methodology is now applied via simulations to a small MV grid. At the end of this section, we also present preliminary localization results to illustrate the impact of the identified insensitivity range.

TABLE I
LIST OF THE SCENARIOS THAT ARE INVESTIGATED IN THE SENSITIVITY ANALYSIS.

Scenario	Parameters	Initial Values	Scaling Factors
Loads	Active power (kW) and inductive reactive power (kvar) [P,Q]	depend on location, e.g. (100,50)	(1.0, 1.0), (0.25, 0.25), (0.5, 0.5), (2.0, 2.0), (4.0, 4.0), (1.0, 0.25), (1.0, 0.5), (1.0, 2.0), (1.0,4.0)
Fault time	Time of fault (s) beginning with maximum voltage at phase 1	10ms	8 steps with $\Delta = 1/8 * 20$ms
Capacitances (jointly c1 and c0)	Positive- and zero-sequence capacitances (μF/km) [c1, c0]	(0.3, 0.3)	joint scaling with factors: 0.9, 0.95, 0.98, 0.99, 1.01, 1.02, 1.05, 1.1
Inductances (jointly l1 and l0)	Positive- and zero-sequence inductances of lines/cables (H/km) [l1, l0]	(0.4e-3, 1.5e-3)	joint scaling with factors: 0.9, 0.95, 0.98, 0.99, 1.01, 1.02, 1.05, 1.1
Inductances l0	Positive- and zero-sequence inductances of cables/lines (H/km) [l1, l0]	(0.4e-3, 1.5e-3)	scaling of l0: 0.9, 0.95, 0.98, 0.99, 1.01, 1.02, 1.05, 1.1
Cable Resistances r0	Positive- and zero-sequence resistances (Ohms/km) [r1, r0]	(0.2, 1.0)	Scaling of r0: 0.5, 0.75, 1.25, 1.5, 2.0
Petersen Coil	Resistance (Ohms), inductance (H) [r, l]	(1.0, 4.2)	(1.0, 1.0), (0.25, 0.25), (0.5, 0.5), (2.0, 2.0), (4.0, 4.0)
Three-phase voltage source	Short circuit power (MVA)	150	1.0, 0.5, 0.8, 1.2, 1.5

A. Grid Scenario

The grid which is used for fault localization and signal generation is the exact replica selected from a real 30kV MV feeder with 9 MV stations; after 6 MV stations in a radial topology, the feeder forks into two remaining radials. Each MV station in this grid contains a secondary transformer, 30kV to 400V, with a load. Single-phase-to-ground earth faults with parameterizable fault resistance can be injected at any MV station busbar. In total, 9 different fault locations are considered, denoted as B3 to B11 in the subsequent part of the paper.

Figure 3 shows the sample signature created by simulation of the corresponding Matlab/Simulink model. The fault resistance in this example is equal to 10 Ohm and the fault is applied to bus bar B10.

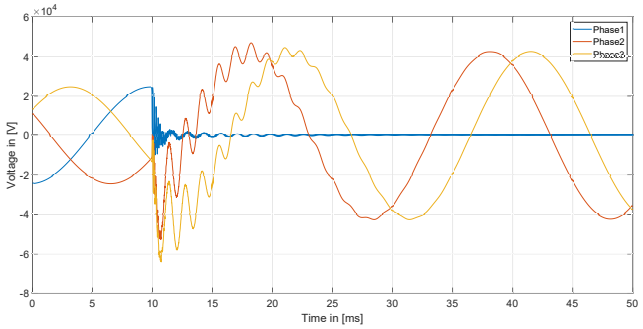

Fig. 3. Signature for fault location B10 and fault resistance 10Ohm, created from the transient simulation of the considered MV grid.

B. Result Visualization

For the purpose of a visual inspection of the impact of different parameter scalings on the signatures, the absolute value of the pairwise correlation coefficient between all the investigated signatures as given in Eq. (2) is used. Figures 4, and 5 illustrate the symmetric correlation matrices with color-coded coefficients. On the lower x-axis, the nine different fault locations are listed. For each fault location, the different parameter scalings as listed in Table I are repeatedly applied, e.g. in the loads scenario, we have nine different scaling factors for each of the nine different fault locations resulting in 81 correlation coefficients per row.

C. Sensitivity to Load Changes

In the first experiment, we show the influence of varying active and reactive power, i.e. the loads associated to each substation. The upper part in Figure 4 shows the matrix representing the pairwise correlation coefficient between all generated signatures, assuming a 0 Ohm fault resistance. The resulting block structure indicates that parameter changes concerning the loads do not impact the correlation coefficient within each fault location (intra correlation). Even more, the correlation between signatures from different fault locations (inter correlation) remains lower than the intra correlation coefficients. The outcome of the same experiment with different fault resistances of 10 Ohm and 100 Ohm have been computed, too. The correlation coefficients in the case of 10 Ohm fault resistance are shown in Figure 4 in the lower part. Although the range of the correlation coefficients gets smaller, the same behavior can be observed, rendering the proposed signature localization approach reasonable. Therefore, loads do not need to be measured accurately, as the voltage signatures with the applied data preparation are robust to load changes.

D. Sensitivity to Cable/Line Parameters

Another source of changes in the signature characteristics are the cable parameters, primarily the positive- and zero-sequence capacitances and inductances. Figure 5 exemplarily illustrates the correlation coefficients obtained after varying the cable capacitances. In contrast to previous results, the impact

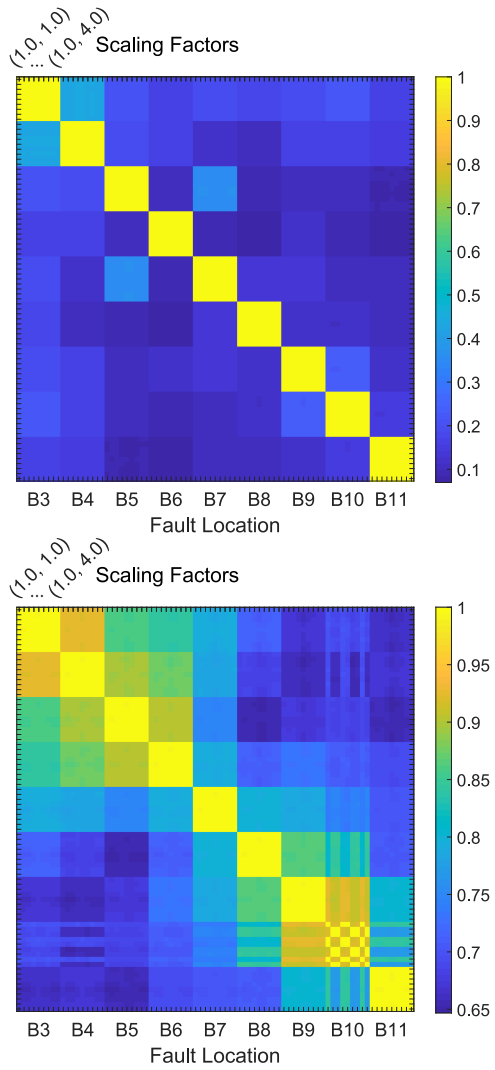

Fig. 4. Correlation coefficient assuming varying active and reactive power of the loads. Top: Fault resistance 0 Ohm. Bottom: Fault resistance 10 Ohm.

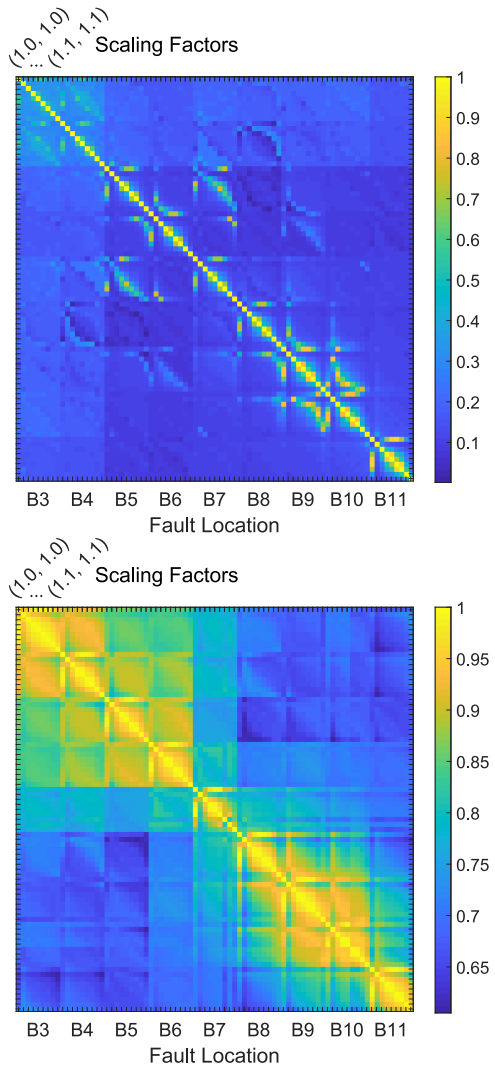

Fig. 5. Correlation coefficient assuming varying cable capacitances. Top: Fault resistance 0 Ohm. Bottom: Fault resistance 10 Ohm.

of these parameters on the signatures is significantly higher, which can be easily seen due to the missing block structure.

E. Summary of the Analysis

In order to allow for an objective evaluation we also assess the sensitivity according to the metric introduced in Sect. III-C. The threshold used to identify the insensitivity range is set to 0.9, i.e. we consider a signature to be robust against parameter changes if at least 90% of the signatures from other fault locations exhibit a lower correlation coefficient with regard to the one generated with the true parameter setting. Table II lists the range of scaling factors, that lead to signatures which fulfill the aforementioned conditions and thus are within the insensitivity range. The range is listed for different fault resistances separately as illustrated in columns two to four. For example, the interval $[0.25, 4.0]$ indicates that a scaling of the corresponding parameters within this range still leads to signatures who can be robustly assigned to the right fault location.

The table shows that there is a wide insensitivity range for loads, fault time (with some exceptions when the faulty-phase transient voltage is close to zero at the time of fault), line/cable resistances r0, Petersen Coil parameters and modeling parameters of the HV grid representation (power source). On the other hand, line/cable capacitances, and inductances need to be accurately determined within some 2% to 5% in order to make the localization approaches with the described data preprocessing and signature comparison method work. A preliminary assessment using the same sensitivity analysis approach on a larger realistic MV grid with 87 stations and many branches confirms similar insensitivity ranges; the case of varying cable/line inductances even shows a slightly larger insensitivity range in this larger grid scenario. Results of this detailed study of larger scenarios will be presented in future work.

TABLE II
INSENSITIVITY RANGE FOR PARAMETER VARIATIONS IN DIFFERENT SCENARIOS AND FOR DIFFERENT FAULT RESISTANCES

	Fault resistance		
Scenario/ parameter	0 Ohm	10 Ohm	100 Ohm
Loads	[0.25, 4.0]	[0.25, 4.0], except fault location B10, there [1.0, 4.0]	[0.25, 4.0]
Fault time	insensitive	sensitive to time of fault close to zero crossing of voltage	
Capacitances (jointly c1 and c0)	[0.98, 1.02]	[0.95, 1.05]	[0.98, 1.02]
Inductances (jointly l1 and l0)	[0.98, 1.02]	[0.95, 1.05]	[0.98, 1.02]
Inductances l0	[0.95, 1.05]	[0.9, 1.05]	[0.95, 1.05]
Resistances r0	[0.5, 2.0]	[0.5, 2.0]	[0.5, 2.0]
Petersen Coil (R and X jointly)	[0.25, 4.0]	[0.25, 4.0]	[1.0, 4.0]
Three-phase source, Short circuit power	[0.5, 1.5]	[0.5, 1.5]	[0.8, 1.2]

TABLE III
PRELIMINARY LOCALIZATION RESULTS BASED ON EARTH FAULTS GENERATED WITH VARYING CABLE/LINE INDUCTANCES.

Scaling factors (jointly l1 and l0)	0.9	0.95	**0.98**	**1.02**	1.05	1.1
Accuracy	0.44	0.89	**1.00**	**1.00**	0.78	0.44

F. Preliminary Localization Results

This section makes a preliminary assessment of the impact of parameter variations on the localization accuracy. Fur this purpose, we generated signatures with different fault resistances, namely $0, 2, 5$, and 10 Ohm, at each of the 9 potential fault locations in our grid. The latter form our signature database for localization. The parameters for the grid are set to the initial values.

In the testing phase, earth faults are simulated with a fault resistance of 1 Ohm and we vary the inductances of the cables/lines as given in the fifth row of Table I. The test signal that is that way generated is now compared to all samples in the signature database, using the correlation metric as introduced in section III-B. The fault location from the signature with the highest correlation to the test signal is used as the estimated location of the fault. The accuracy in Table III is given as the percentage of correctly identified fault locations over the 9 runs for different true fault locations.

The results confirm the insensitivity range given in Table II, since an accurate localization of the 9 earth faults is observed in the table only when the cable/line inductances used for the test data generation is within the identified insensitivity range.

V. CONCLUSION AND OUTLOOK

This work has analyzed the robustness of the signature based Earth Fault Localization from [9] towards parameter changes. The results show that within the investigated parameter ranges, the localization approach using correlation for signature comparison is robust to load changes and to changes of the time of fault. Cable inductances and capacitances on the other hand have a strong influence. To mitigate the impact of influential parameters on the signature generation phase, three basic approaches can be applied: (1) Improve the quality of the used parameters, e.g. via estimation from additional live measurements. This however comes at extra cost of measurement infrastructure. (2) Include variations of the influential parameters in the signature database. In a preliminary experiment extending the scenario of Table III, such approach was successful, however, it increases the effort for signature creation; in particular in case of cable/line parameters (where some tens to hundred cables or lines are part of the grid model), parameter variations can lead to a combinatorial explosion of the signature space. (3) Modify the data preprocessing or the signature comparison approach to become robust to the sensitive parameter. Future work will investigate the actual localization accuracy using measurements from live MV grids and further research will investigate the three mitigation approaches introduced above.

REFERENCES

[1] T. S. Abdelgayed, W. G. Morsi, and T. S. Sidhu. Fault detection and classification based on co-trainingofsemisupervisedmachine learning. *IEEE Transactions on Industrial Electronics*, 65(2):1595–1605, 2018.

[2] F. Carlsson, N. Etherden, A.K. Johansson, D. Wall, A. Fogelberg, and E. Lidstrm. Advanced fault location in compensated distribution networks. In *IET Conference Proceedings*, 2016.

[3] K. Chen, C. Huang, and J. He. Fault detection, classification and location for transmission lines and distribution systems: a review on the methods. *High Voltage*, 1(1):25–33, 2016.

[4] Y. Chollot, J. Mecreant, D. Leblond, and P. Cumunel. New solution of fault directional detection for mv fault passage indicators. In *24th International Conference and Exhibition on Electricity Distribution (CIRED)*, June 2017.

[5] M. Farshad and J. Sadeh. A novel fault-location method for hvdc transmission lines based on similarity measure of voltage signals. *IEEE Transactions on Power Delivery*, 28(4):2483–2490, October 2013.

[6] A. Farughian, L. Kumpulainen, and K. Kauhaniemimi. Review of methodologies for earth fault indication and location in compensated and unearthed mv distribution networks. *Electric Power Systems Research*, January 2018.

[7] H. Jingguang, H. Xiangyong, L. Xianshan, H. Hanmei, and L. Yanping. A novel single-phase earth fault feeder detection by traveling wave and wavelets. In *International Conference on Power System Technology*, 2006.

[8] H. Livani and C. Y. Evrenosoglu. A machine learning and wavelet-based fault location method for hybrid transmission lines. *IEEE Transactions on Smart Grid*, 5(1):51–59, 2014.

[9] H.-P. Schwefel and N. Silva. Ep3553541b1: Device and method for locating earth faults in electrical distribution grids, September 2020.

[10] N. Silva. Griddata Newsletter February 2019, 2019. URL: http://www.griddata.eu/NL02_ENG/190227_GridData_Newsletter_February_ENG.pdf.

[11] J. Yang, J. E. Fletcher, and J. O'Reilly. Short-circuit and ground fault analyses and location in vsc-based dc network cables. *IEEE Transactions on Industrial Electronics*, 59(10):3827–3837, 2012.